Supplementary Information
for
Stretchable Touch-Sensing Skin over Padding for Co-Robots

Ying Chen, Miao Yu, Hugh A Bruck, and Elisabeth Smela

1 Testing of EG/Latex Sensing Film Alone

The piezoresistive sensing material is an EG/latex composite, meaning that it is also viscoelastic [60]. It was therefore separately characterized to understand its temporal responses in the absence of the underlying membrane. The sensing material was applied as a thin adherent film – too thin to be peeled off and handled alone – so it was characterized on a stiff bending cantilever as described in [49]. This limited the range of strains to a maximum of 1500 microstrain (με). The free end of the cantilever was displaced by known distances with step and sinusoidal inputs to obtain the static and dynamic responses.

1.1 Method

The EG/latex sensing material was applied on two cantilevers (Lexan polycarbonate, 27 mm wide x 185 mm long x 2 mm thick) by spray coating. The dimensions of the sensors were 7 mm x 25 mm. Electrical connections were made following the method described in Section 2.1.3 of the main text.

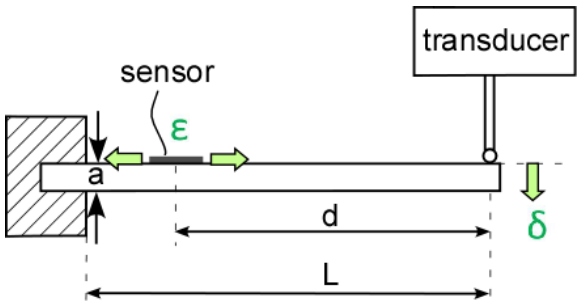

Figure 15. Schematic for testing the EG/latex sensor alone. The cantilever tip displacement δ and the strain ε are indicated for tension. For compression, the cantilever was flipped over. (L = 155 mm, a = 2 mm, d = 135 mm.)

The end of the cantilever close to the sensor was rigidly clamped. The free end was displaced to induce either tensile (face up, as shown in Figure 15) or compressive (face down) strain using a programmable force transducer (Bose 3330 Series II). Using small angle beam theory, the relation between the tip displacement δ and the strain ε at the center of the sensor is given by:

$$\varepsilon = \frac{3da}{2L^3}\delta, \quad (1)$$

where L is the length of the cantilever, d is the distance from the center of the sensor to the end of the cantilever, and a is the cantilever thickness.

1.2 Calibration

The change in resistance was measured in both tension and compression. The cantilever tip was displaced to 8 positions for each (producing strains in the sensor of ±0.01, ±0.02, ±0.03, ±0.04, ±0.09, ±0.13, ±0.17, and ±0.22 %), in increasing order to a maximum strain of 2200 με = 0.22%. Each position was held for 2 seconds, and the resistance was measured immediately after the deflection was reached: due to the relaxation behavior of the composite, shown below, a steady-state value could not readily be identified.

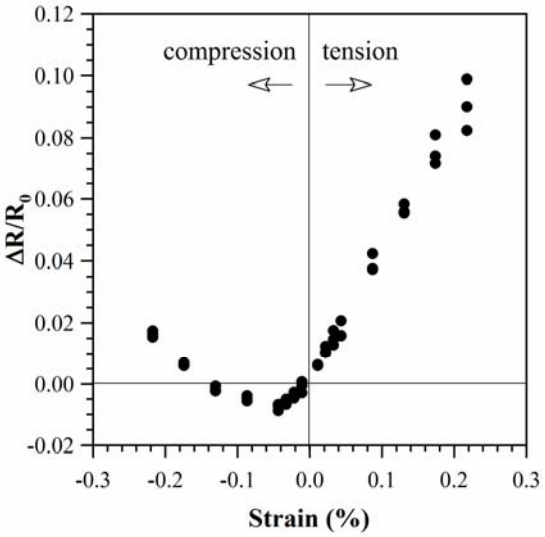

Figure 16. Relative resistance change as a function of strain. Data from triplicate measurements are shown for one of the cantilevers.

The static response is shown in Figure 16 for one cantilever; the behavior was identical on the second one. The sensitivity under tension and compression differed. Under tension the resistance increased linearly with the strain, as previously found in [20].

Under compression, the response was non-monotonic, decreasing at small compressive strains (up to -0.05%), and thereafter climbing. Prior reports have shown that the response under compression is highly sensitive to particle loading and shape, as discussed in [49].

1.3 Relaxation and Recovery

Viscoelasticity is typical for elastomeric polymer composites. To understand the performance of our EG/latex sensor, relaxation and recovery tests were also conducted on the cantilever. The sensor was rapidly placed under tension, 0.05% strain, by displacing the cantilever tip at a speed of 15 mm/sec and then holding that position for 200 sec while recording the resistance. (An

ideal step input is not achievable experimentally. At rates faster than 15 mm/sec, vibration is introduced.) The strain was then released by retracting the cantilever tip at the same 15 mm/sec, and the recovery process was monitored for 100 sec.

The strain waveform and the resistive response are shown in Figure 22 in Section 3.2 (left *y*-axes, black curves). The resistance changed immediately with the strain, but after that, due to the re-arrangement of the host polymer chains and guest particles, the resistance decreased gradually. When the strain was released, the resistance recovered back to its initial value, without suffering a permanent residual resistance change.

The relaxation of the resistance is related to viscoelastic stress relaxation [60]. Relaxation in polymer composite sensors has been investigated previously [16,41,61], with relaxations times of hundreds of seconds, comparable to our EG/latex sensor. This phenomenon does not prohibit applications in strain sensing application, as shown in [15,25,42].

1.4 Cyclic Loading

To investigate the sensor response to cyclic loading, a sinusoidal displacement was applied to the tip of the cantilever using the same apparatus. The results for a tip displacement to 5 mm at 1 Hz are shown in Figure 17. The change in resistance was the same at 0.1 Hz and at 9 Hz, as previously shown in [49]: the sensor is able to respond quickly to the AC input because it is faster than the much slower viscoelastic (rubbery) response shown in Figure 22, which persists for hundreds of seconds. At these frequencies, the polymer behaves substantially as a glassy material.

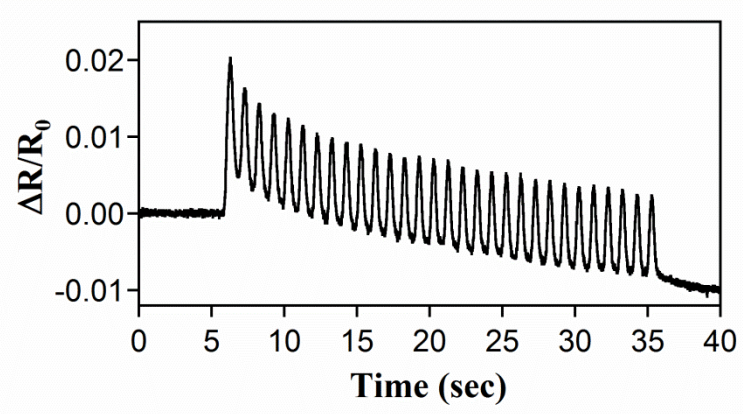

Figure 17. Relative change in resistance due to a sinusoidal cantilever tip displacement of 5 mm starting at t = 6 sec.

2 Calibration of the Sensor on the Membrane

The sensitivity of each sensor to tensile strain was calibrated. The experimental configuration used for the uniaxial tensile testing is shown in Figure 18. The sensors were suspended vertically and stretched to different positions, defined by shims of known thickness. The

reference sensor was stretched to 5 positions, stretching the 90 mm initial length by 2.5, 5, 10, 15, and 20 mm (3.2, 6.5, 13.0, 19.5, and 26.0%, respectively). The 15 sensors used in the loading tests were stretched by 3% and 6%, and linear curve fits were used to obtain the gauge factors. Calibrations were conducted in triplicate. The gauge factors for all 15 sensors are shown in Figure 19. The gauge factors of the other 14 sensors were normalized to that of sensor #1.

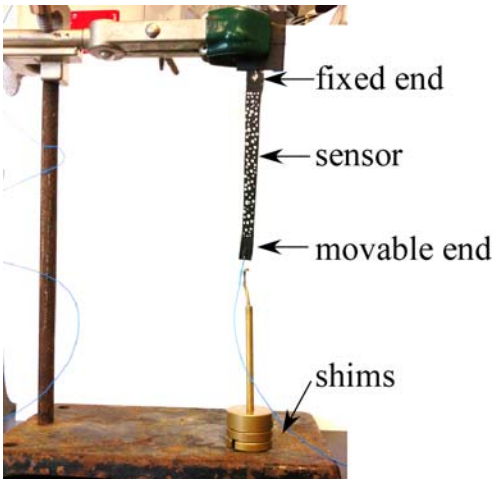

Figure 18. Experimental setup for tensile calibration of the EG/latex sensor+membrane samples. (The white speckling was for DIC strain measurements.)

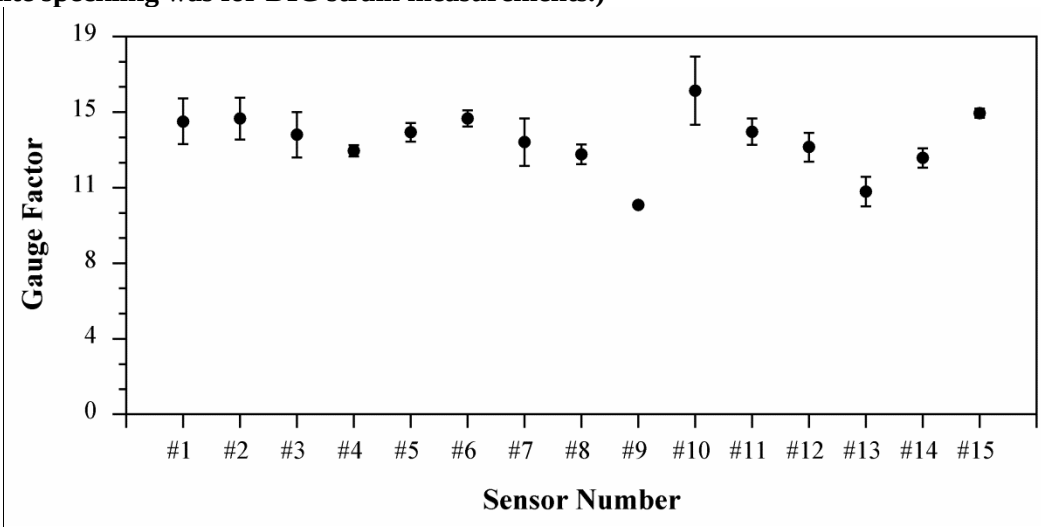

Figure 19. Gauge factors for the 15 sensors used for load testing. Measurements were performed in triplicate; points show the average and error bars the standard deviation.

The performance of the sensing skin was re-measured by indentation testing after a period of 6 months (Figure 20). The relative change in resistance decreased somewhat, but not substantially.

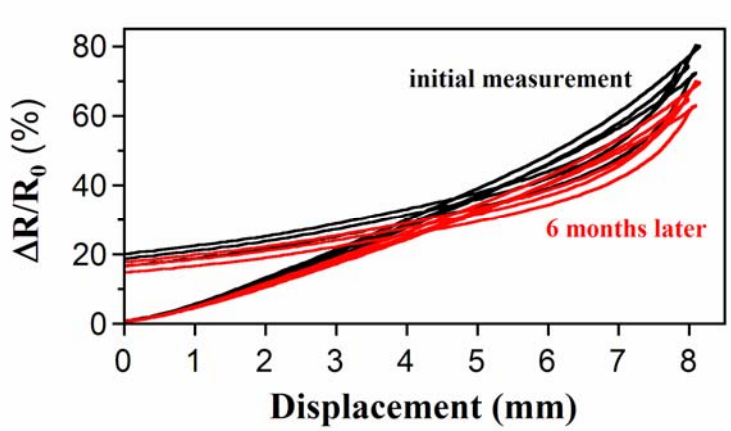

Figure 20. Performance of the sensing skin in indentation tests (3 cycles each) performed 6 months apart.

3 Uniaxial Dynamic Testing of Sensor on the Membrane

To further examine the behavior of the sensing skin (sensor + membrane), dynamic uniaxial tests under both static and cyclic loading were performed.

3.1 Method

Strip-shaped sensor skins fabricated as described in Section 2.1 was mounted as shown in Figure 21. The two ends, including the electrical connections, were clamped to blocks. The bottom block was fixed, and the top block was connected in series with the transducer (Bose 3330 Series II) and the load cell (Cooper Instruments & Systems LFS270 5 lbs (2.3 kg)). The skin was strained by moving the top block as programmed by the transducer.

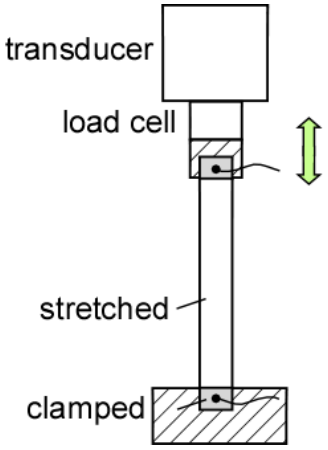

Figure 21. Experimental setup for uniaxial dynamic test of the skin.

3.2 Relaxation and Recovery

The rubber membrane allows a much large strain deformation than a substrate that is only flexible, a significant benefit for a conformal skin. To investigate the effect on the dynamic response of adding the rubber membrane under the sensor, relaxation and recovery were monitored on the skin in response to a step waveform to 4% strain (Figure 22a, right *y*-axis, red curve) using the apparatus shown in Figure 21. The change in resistance is shown in Figure 22b.

The sensing skin again showed the resistive relaxation expected from viscoelastic composites, and the resistance returned fully to its initial value during the recovery phase. The shape of the curve was comparable to that for the sensor alone. This is not surprising, since both the sensor and the membrane were made of latex. Significantly, the membrane did not slow down the sensor response.

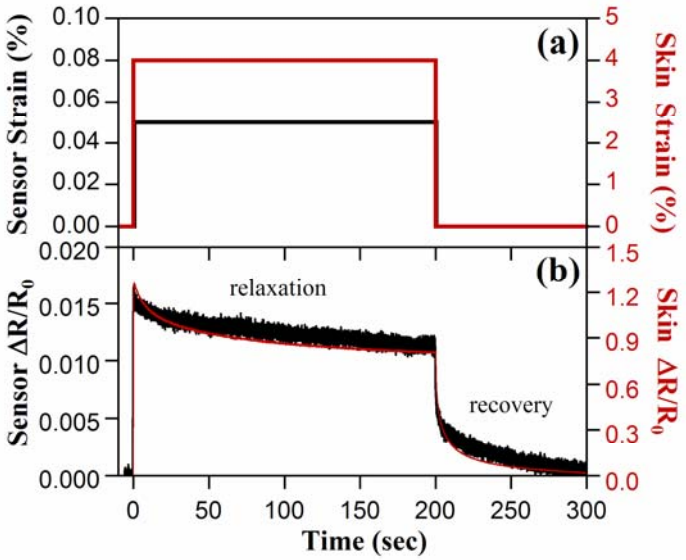

Figure 22. Relaxation and recovery of the sensor on the rigid bending cantilever and on the rubber membrane. (a) Strain waveforms. For the cantilever, a constant strain of 0.05% was applied (relaxation) and released back to 0% (recovery). For the membrane, a strain 4% was applied and released. (b) Resistance response of the EG/latex on the cantilever (left *y*-axis) and the rubber membrane (right *y*-axis).

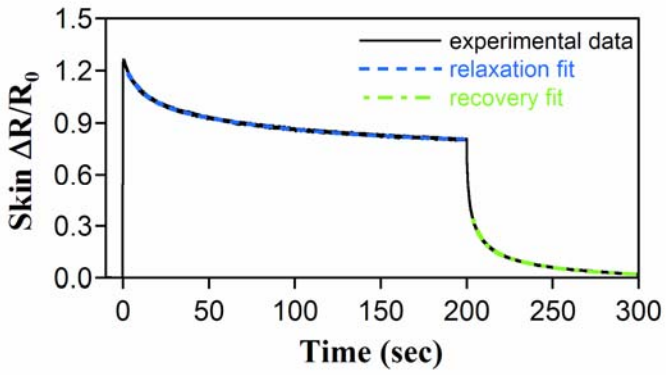

Figure 23. Experimental step response data and fitted curves.

To determine the time constants of the skin during relaxation and recovery, we employed a Generalized Maxwell or Maxwell-Wiechert model with two time constants, fitting the relaxation and recovery responses separately. The models often differ for relaxation and recovery, and can account for variations in the response due to variations in the structure of the material. The resistance response over time was formulated as:

(2) $\Delta R/R_0 = c_0 + c_1 \cdot e^{-t/\tau_1} + c_2 \cdot e^{-t/\tau_2}$,

where $c_0, c_1,$ and c_2 are amplitudes and τ_1 and τ_2 are time constants.

The fits are shown in Figure 23. For relaxation τ_1 = 11 sec and τ_2 = 90 sec, whereas for recovery τ_1 = 6 sec and τ_2 = 37 sec. Note that these are not comparable to the recovery time in the main text (Figure 8), which was found differently. In [16,41,61], the sensors had relaxation times on the order of a hundred seconds.

3.3 Uniaxial Cyclic Loading

We investigated the sensing skin response to cyclic loading to compare it with the cyclic response of the skin over padding (Section 3.4.2). A 30-cycle sinusoidal uniaxial strain at a frequency of 0.2 Hz was exerted on the skin. The maximum strain was 4%, equivalent to the maximum strain experienced in the indentation tests over the padding.

The force response is shown in Figure 24a; it did not change significantly over the 30 cycles. The skin maintained the same amount of hysteresis, meaning that it dissipated the same amount of energy in each cycle. The response stabilized after the 2nd cycle, which was also the case for indentation over padding (right side, part (d)). However, over padding the shape of the first loop was different from the subsequent 29 cycles, showing that more energy was dissipated in the first cycle. The padding dominated the behavior in Figure 11, which is also clear from the 10x larger force amplitude.

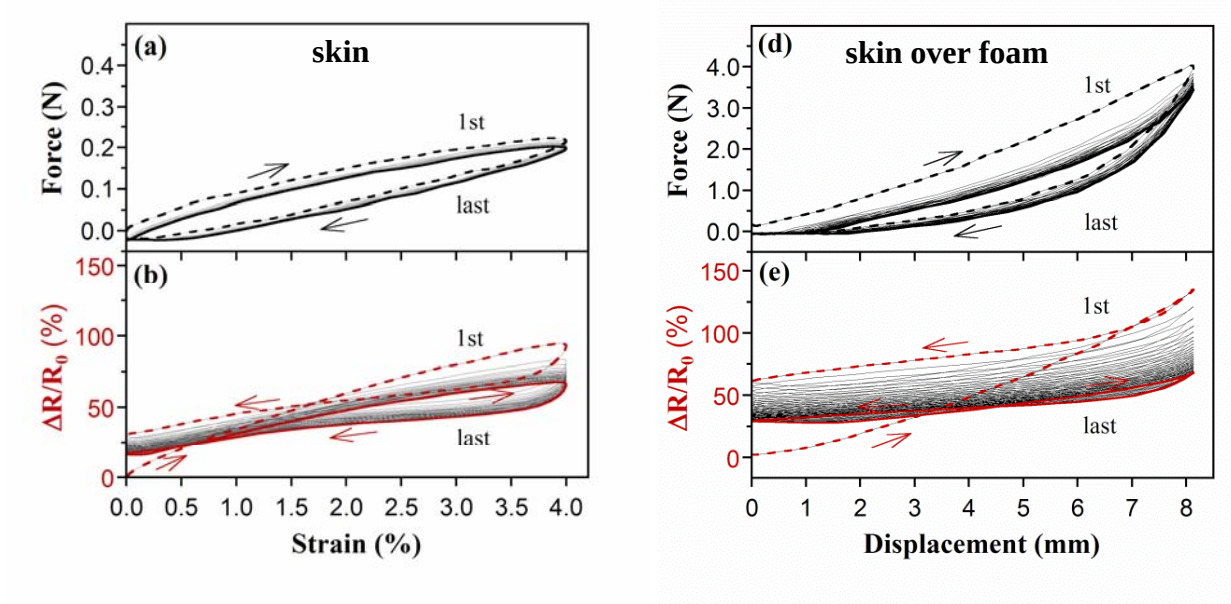

Figure 24. (left) Sensor+membrane in cyclic tests. The input strain waveform was a 30 Hz sinusoid. (a) Force and (b) normalized resistance change versus strain. (First cycle, dashed line; last cycle, heavy solid line.) (right) Right half of Figure 11 Error! Reference source not found. **showing the corresponding data from the skin over the foam. Note the differences in the axis values.**

In Figure 24b, the resistance changed in a similar manner as for indentation over padding (compare Figure 11e), showing a figure-8 shaped loop. The 1st cycle showed an irreversible resistance increase upon unloading. After that, the end-of-cycle resistance shifted toward a stabilized position. Over the 30-cycle loading, the hysteresis remained the same, but it was larger than in the indentation tests (Figure 11e).

4 Biaxial Tensile Testing of Sensing Skin

To more closely approximate the deformations experienced in the indentation tests (Figure 5b), which are not unidirectional, biaxial testing was performed to determine whether the sensitivity in the *x*-direction was affected by strain in the perpendicular *y*-direction (or lateral direction). The results showed that it is not: *the slope of the curve in the x-direction is unaffected by amount of stretching in the y-direction*. This means that the sensor is able to maintain the same sensitivity when lateral strain exists, which is a good attribute for multi-axial deformation measurements.

4.1 Fabrication

Biaxial tensile testing was performed on a cruciform-shaped sensor prepared using the same method as the strip-shaped sensor. The geometry of the cruciform-shaped specimen is shown in Figure 25. The cruciform shape was formed on the latex membrane sheet (again from ELE International, 0.3 mm thick) by a stencil created from painter's tape (ScotchBlue). As with the

other samples, the piezoresistive paint was applied by spray-coating onto the latex membrane (10 psi air pressure) in a hood and allowed to air dry for one minute, repeating to deposit 10 layers. After spray coating, the pattern was scissor cut along the boundary to create the cruciform-shaped specimen. Connecting wires (single strand, 30 AWG) were attached with silver epoxy (CircuitWorks, CW2400) between points 1 and 3 in Figure 25. The four ends of the specimen (including the portions with the attached electrodes) were glued (Aleene's fabric glue) to the tops of the four arms of a biaxial testing rig, giving a stretchable length of $L_x = L_y = 30$ mm in both the x and y directions. The fixed and stretchable area of the specimen are color coded in Figure 25.

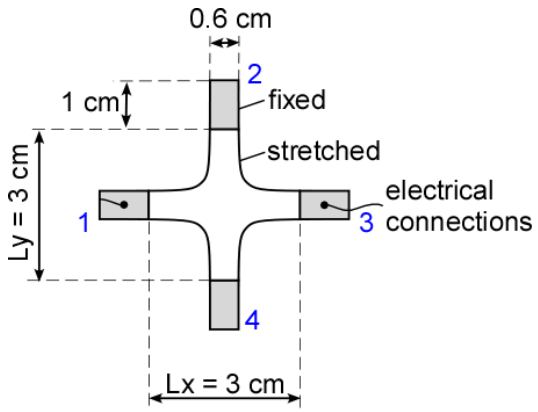

Figure 25. Dimensions of the cruciform-shaped sensor. The fixed part is indicated by the shaded area, and the stretchable part by the white area. The resistance was measured between the points 1 and 3.

4.2 Experimental Setup

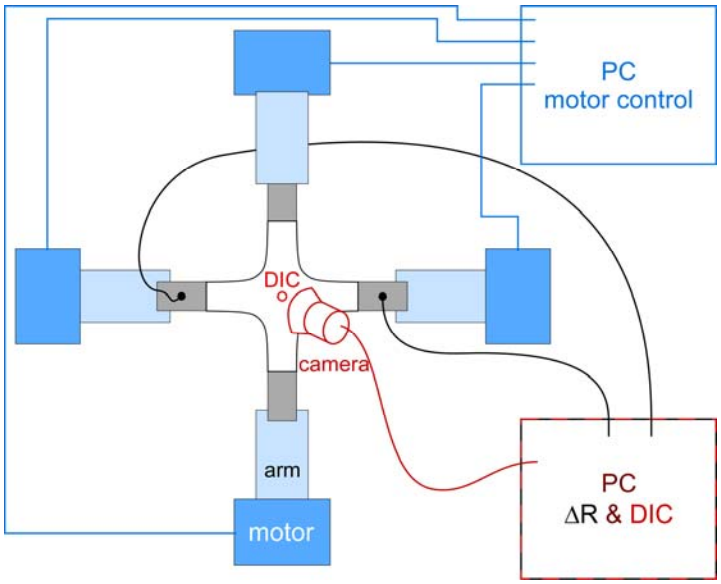

Figure 26. Schematic diagram of the biaxial tensile testing setup. Note that the camera is looking straight towards the DIC area (red circle).

The movement of the arms was driven by four independent, linear, pneumatically-driven motors controlled by program written in LabVIEW. The resistance and local strains were measured simultaneously. In order to see the effect of lateral strain, the resistance was measured between points 1 and 3 (*x*-direction in Figure 25) across the whole sample, and lateral strain was applied in the perpendicular *y*-direction. Figure 26 shows an overhead view of the setup.

Local strains were obtained from two dimensional digital image correlation (2D-DIC) [52-55], which gives inplane strain information. The surface of the sensor was painted with random speckles (Rust-Oleum Quick Color aerosol paint, white; speckle size 0.02~0.24 mm dia.). One camera was positioned to look perpendicularly toward the sample and was focused on a 1 mm x 1 mm area. 2D-DIC software (Vic-Gauge 2D, Correlated Solutions) was used to collect and analyze the images and obtain the strain information.

4.3 Results

The inset in Figure 27b shows where the local strains were measured using 2D DIC in the center of the sample (indicated by the red circle). Note that the local strains in the *x*- and *y*-directions differ and vary across the sample, and they are not the same as the global strains between the motorized arms. Strains at the center were highest and decreased to zero at the fixed ends of the arms, as confirmed by DIC at those positions (black circles in Figure 27b inset). Also note that the resistance was measured across the whole sample.

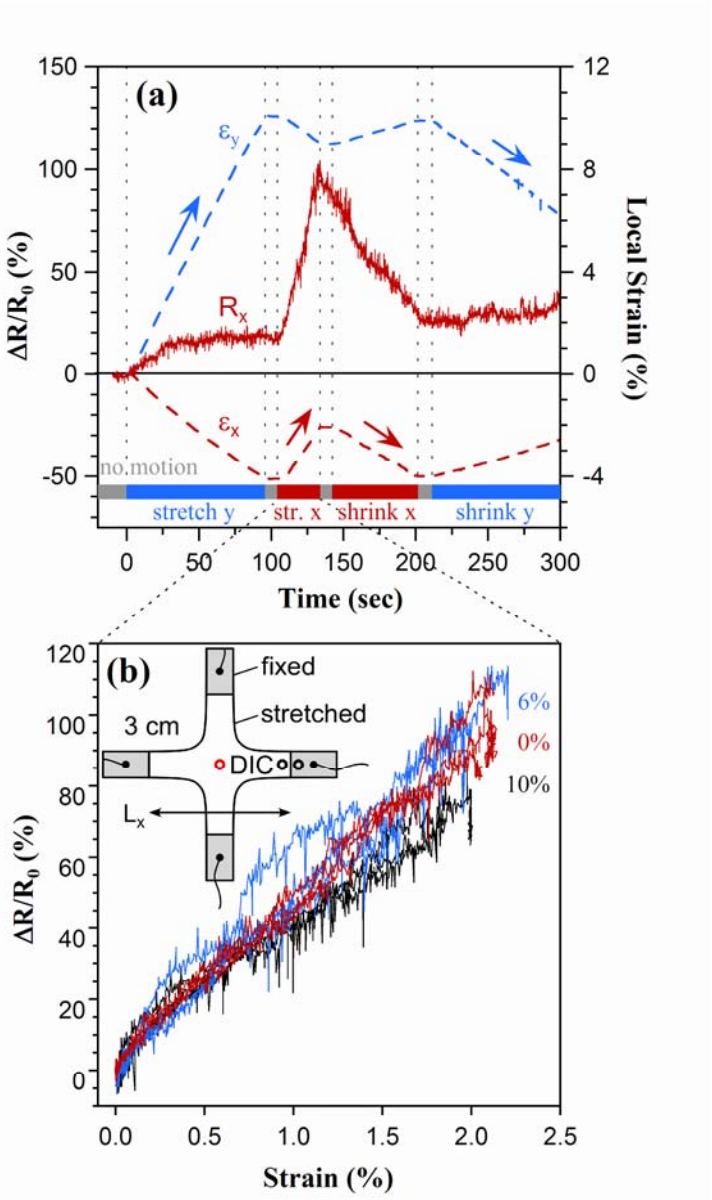

Figure 27. a) Local strains ε_x and ε_y (dashed lines) obtained from DIC in the center of a cruciform specimen (red circle in inset in (b)) and normalized change in resistance (global) in the *x*-direction over time as the sample was sequentially stretched in *y*, stretched in *x*, relaxed in *x*, and relaxed in *y*. b) While *y* was kept fixed and *x* was stretched, the change in normalized resistance in the *x*-direction as a function of ε_x for three different ε_y, in triplicate. The starting points of all the curves were aligned at (0,0).

The experimental procedure is illustrated by the color-coded bar at the bottom of Figure 27a. The sample was stretched (for approximately 100 seconds, blue bar on legend) in the *y*-direction until the local strain ε_y in the center of the sample (dashed blue line, right axis) reached 10%. At the same time, the local strain in the *x* direction, ε_x (dashed red line, right axis), decreased by Poisson's ratio. This position was next held a few seconds (gray on legend), stretched in the *x*-

direction to a local strain increase of ε_x = 2%, held again, released in *x* back to the original position, held, then released in *y*. The sequences were run in triplicate at three values of ε_y, 0%, 6%, and 10%. The normalized change in resistance between points 1 and 3, R_x (solid red line, left axis), is also shown.

The three curves in Figure 27a show the relative resistance change in the *x*-direction, as well as the local strains ε_x and ε_y in both the *x* and *y*-directions induced by the lateral stretching. Although globally there was no strain along the *x* direction, the local strain ε_x decreased by 4% due to Poisson's ratio as the *y*-direction was stretched. When stretching *y*, R_x initially increased with ε_y, but it plateaued at 17% (Figure 27a). This also occurred for the measurements at 6% and 10% lateral strains. Since the sensing material covers the entire cruciform shape, strain within the sample can change the percolation pathways and thereby the resistance along the conductive paths. However, it is not clear why R_x increased only initially and then plateaued.

Once the central local strain in *y* was fixed at ε_y = 10%, the motor in the *y*-direction stopped stretching the specimen. Then the motor in the *x*-direction started to stretch the specimen until the central local strain ε_x increased by 2% from its starting value. During this period, R_x rose to nearly 100%, and ε_y decreased by 1%. Upon reducing ε_x, R_x decreased again. R_x was more sensitive to strain in *x* because that affected the entire length of the strain gauge in the *x* direction, whereas strain in *y* affected only the center (and the arms connecting points 2 and 4.)

Calculating a gauge factor based on local strain, $GF = R_x/\varepsilon_x = 41$, nearly 3 times the value of 14 found in the uniaxial tests. This is reasonable because the resistance was measured over regions where the strain was much lower than the local strain at the center of the sample. Results from the second sample were similar.

Figure 27b shows the change in resistance in the *x*-direction, R_x, as the sample was stretched up to ε_x = 2% (local strain in the *x*-direction). Three lateral strains (ε_y = 0, 6, and 10%) were applied to investigate their effect on the sensitivity. Triplicate measurements at each ε_y are plotted in the same color. (To facilitate comparison, the $\Delta R/R_0$ value of the 6% and 10% curves have been shifted downward by 17%, and the strain shifted by +3% and +4% respectively, so that they all have the same starting point.) R_x increased linearly with ε_x in all cases. *Most importantly, there was no notable dependence of the slopes on ε_y, so there are no evident nonlinear inplane cross-axis interactions in this range of strains.*

4.4 Discussion

The independence of the slopes in Figure 27b on strain in the perpendicular direction shows that cross-axis interactions on the stretchable sensing skin were small: the gauge factor was substantially unaffected by strain at 90°, even for strains at the center of the sample as high as10%. Strains in the *x* and *y*-directions can therefore be evaluated independently, based on the measurement direction for the resistance.

5 Effect of Coating

Three coatings were tested for their ability to provide abrasion protection for the sensor while not negatively impacting performance: Behr Premium Plus Ultra, Kryolan Flexible Sealor Makeup, 1481, and Zensser, Bulls Eye 1-2-3 Plus Primer. The uncoated sensors were smooth, as shown by the close-up photographs in Figure 28. The Behr paint was viscous, as shown by the brush streaks, and it contained some small particles. It adhered well. The Kryolan coating was transparent and rendered the surface shiny; it also adhered well. The Zinsser primer coating had an inconsistent thickness and small bubbles. Stretching the sensors resulted in cracking and flaking off of the Zinsser coating.

Nine strip sensors were made from one batch of latex/EG, and their sensitivities were obtained as described above. As shown in Figure 28, all nine sensors had similar gauge factors before coating. The sensors were coated and left to dry for 12 hours, and the sensitivity of each sensor was re-measured.

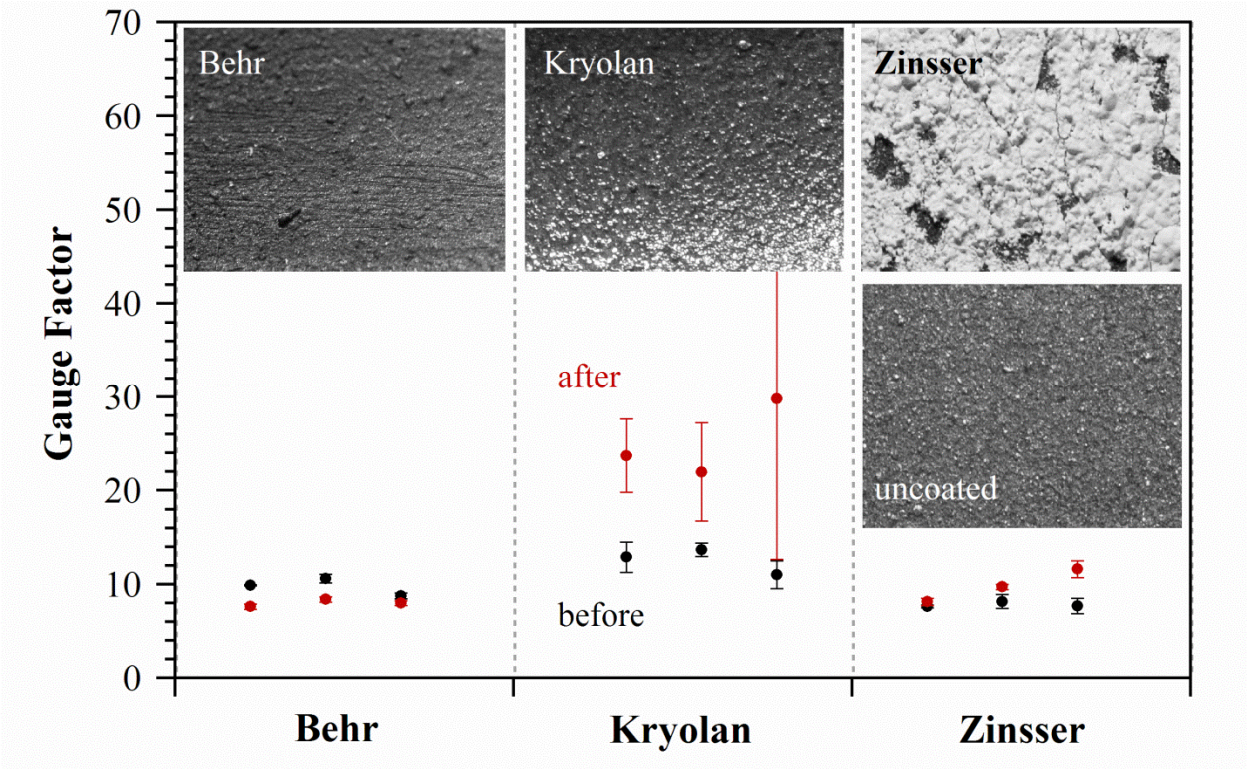

Figure 28. The effect of the coating material on sensor appearance and sensitivity. The gauge factor before (black) and after (red) coating the sensors is shown, and the standard deviation of three replicates is indicated by the error bars. The vertical scale for the photographs is 8 mm.

Sensors coated with Kryolan experienced the largest change: the gauge factors increased, but had a large standard deviation. This was due to the high stiffness of the Kryolan coating, which cracked upon stretching and tore the sensing material, leading to a large signal change. Because such cracks in the coating are uncontrollable, the signal change was inconsistent.

The Behr and Zinsser paints were better coating materials since the gauge factors did not change much. However, there were large particles in the Zinsser coating that lead to a rough surface, and the material flaked off with mechanical contact. In contrast, the Behr coating was smooth and capable of insulating the sensing material from conductive contacts. Therefore, the Behr coating was selected for this study.

6 Loading Rate Dependence

Three probe loading/unloading rates were examined. The data in the main text were from the slowest rate, 0.1 Hz (approx.2.5 mm/sec). Results on foam OC-2 and PDMS-1 are shown in Figure 29. Neither the force nor the change in resistance showed a marked dependence on loading rate in the studied range for any of the padding materials. (The normalized resistance had less time to recover at the faster rates, so the value upon returning to zero displacement was higher, but the maximum change in resistance was the same.)

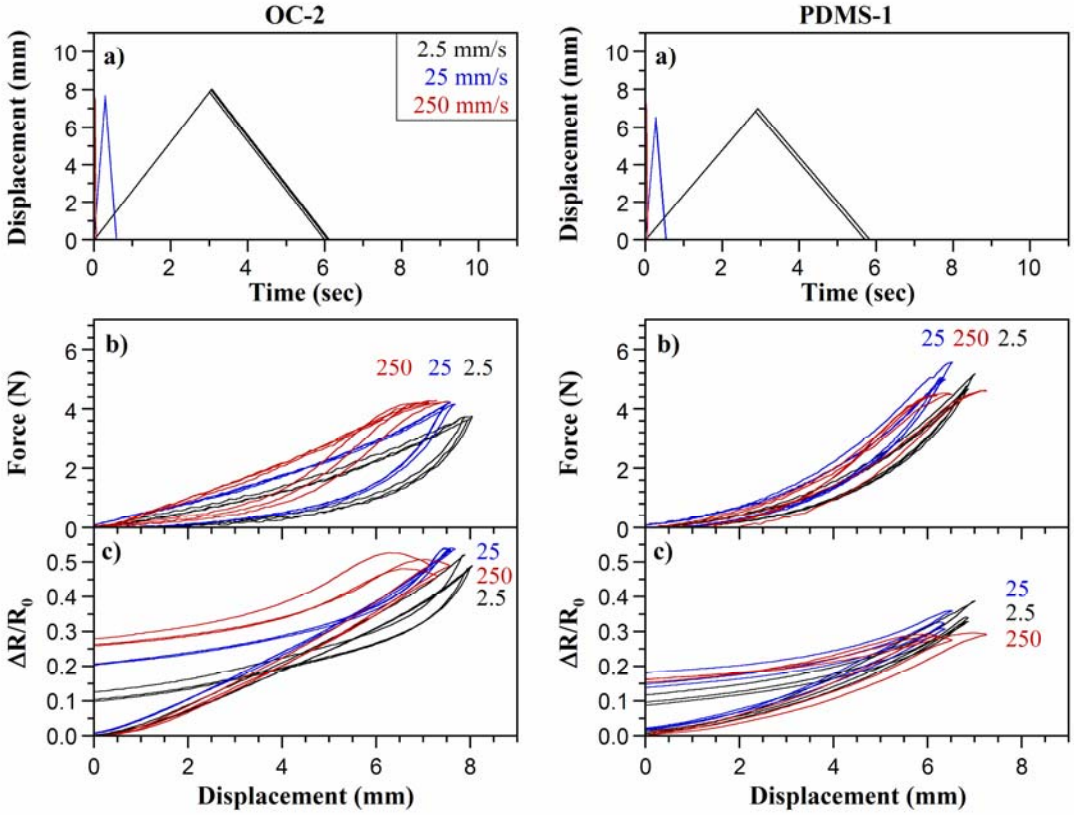

Figure 29. (a) Displacement versus time at three loading-unloading rates: 2.5 mm/s, 25 mm/s, and 250 mm/s (frequency = 0.1 Hz, 1 Hz, and 10 Hz, respectively). b) Force and c) normalized resistance change as a function of displacement at the three indentation rates. For each padding, triplicates on one sensor are shown.

7 Recovery Time

Figure 30 shows the change in resistance over time as the probe indented the skin on the various padding materials (at somewhat varying rates) and then lifted off (as in Figure 8). There was no substantial difference in overall behavior. (The apparent slower response of CC is due to the slower probe motion.) One difference to note is the large variation on PDMS-2.

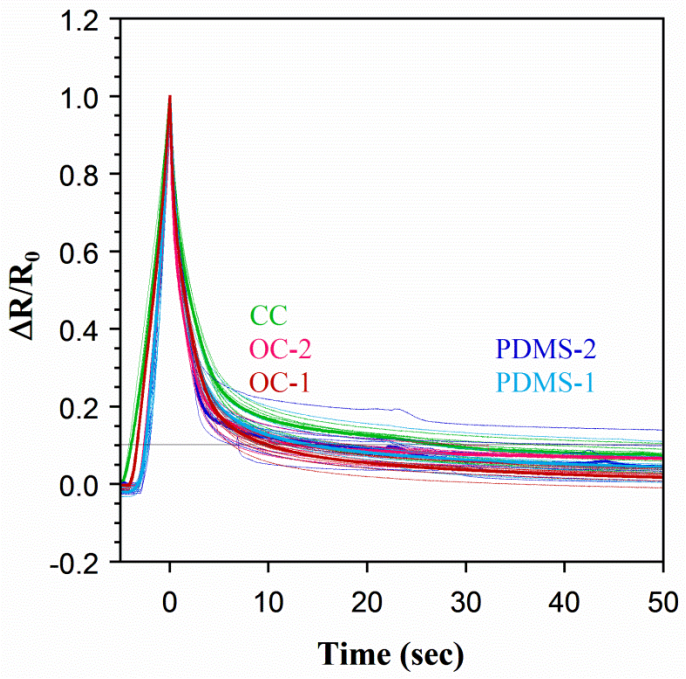

Figure 30. Change in resistance as a function of time on the various padding materials. All 9 curves for each material are shown.

References

60. P. Kelly, University of Auckland, "An introduction to solid mechanics: viscoelasticity", http://homepages.engineering.auckland.ac.nz/~pkel015/SolidMechanicsBooks/, 2015.

61. J. Kost, A. Foux, and M. Narkis, "Quantitative model relating electrical resistance, strain, and time for carbon black loaded silicone rubber," Polym. Eng. Sci., 34 (21), 1628-1634 (1994).